Uniform Flow Past a Closed Body at Low Reynolds Number Employing a Novel Matching in a Boundary Element Formulation

Bwebum Cleofas Dang[1,2,*], Edmund Chadwick[1]

[1] *School of Computing, Science and Engineering*
University of Salford
Greater Manchester
M5 4WT, United Kingdom.
[2] *Department of Mathematics*
Faculty of Natural Sciences
University of Jos
PMB 2084, Jos Plateau State, Nigeria.
[*] *Corresponding author: b.c.dang@edu.salford.ac.uk*

Abstract

Consider a two dimensional steady low Reynolds number flow past a circular cylinder. A boundary integral representation that matches an outer Oseen flow and inner Stokes flow is given, and the matching error is shown to be smallest when the outer domain is as close as possible to the body. Also, it is shown that as the Greens function is approached, the oseenlet becomes the stokeslet to leading order and has the same order of magnitude error as the matching error. This means a novel boundary integral representation in terms of oseenlets is possible. To test this, a corresponding boundary element code is developed which uses point collocation weighting functions, linear shape functions, two-point Gaussian quadrature with analytic removal of the Greens function singularity for the integrations. The method is compared against various methods for the benchmark problem of flow past a circular cylinder. In particular, the drag coefficient is used for the comparison. The advantage of this method over existing ones is demonstrated and discussed particularly in the Reynolds number range $Re = 1 \sim 4$.

Keywords: Low Reynolds number, Boundary Element Method (BEM), Viscous fluid dynamics, Matched asymptotic expansion.

---

1. Introduction

In biological fluid dynamics, the modelling of the motion of macroscopic and microscopic organisms represented by a generic closed swimming body is important, such as flagellated propelled organisms like spermatozoa [14]. In particular, the far-field effect at a centimetre scale is often required. As a first step in this paper, a new boundary element method is developed that also incorporates the far-field matching for low Reynolds number two-dimensional steady flow [1].

The Boundary Element Method (BEM) can be traced back to the 1960's [2], its numerical implementation was made robust with the advent of computers that aid solving sets of integral equations. Partial differential equations can be solved numerically by many different methods such as the Finite Difference Method (FDM) and the Finite Element Method (FEM) which are domain methods. However, in certain circumstances such as this one, if a boundary integral formulation is available, then a formulation based on this such as the Boundary Integral Method (BIM) [4] has advantages. For example, the formulation is expressed on the boundary and so has one dimension less than the domain methods FDM and FEM, making it faster and more accurate. With the development of quadratures and stable discretization, the evaluation of integrals becomes more accurate and efficient [4].

Studies of slow motion of viscous fluid flow past a body in an unbounded domain dates back to the work of Stokes in 1851 [15]. Because of the difficulty in satisfying boundary conditions both at the cylinder surface and the far-field, Stokes draws a conclusion that such a solution does not exist and this hypothesis was later termed Stokes' paradox. Several analytical studies began to emanate, seeking solution to the Stokes' paradox and this include the approximation given by Oseen [11] solved approximately by Lamb [8], [9], and Imai [6]. However, Oseen's approximation assumes linearisation to the free stream velocity which breaks down on the body boundary. To overcome this, the method of matched asymptotic expansions was presented by Proudman and Pearson [13] and Kaplun [7] and it combines linearisation to Stokes flow in the near-field matched to linearisation to Oseen flow in the far-field region. Experimental studies [17] with different qualitative and quantitative results have also been presented, in particular for the benchmark problem of steady flow past a circular cylinder.

Further to different numerical methods used, Yano and Kieda [19] applied a discrete singularity method to solve a two-dimensional flow by distributing oseenlets, sources, sinks and vortices in the interior of an obstacle with a least square criterion to satisfy the boundary condition. Their result was benchmarked against the analytic results of Lamb [9], Kaplun [7] and the experiment of Tritton [17] for the drag coefficient. It was revealed that when the Reynolds number is below one ($Re < 1$), there is good agreement, but when the Reynolds number is in the range 1 to 4 the analytical results do not align very close with experiment except the numerical studies presented by Yano and Kieda [19]. The analytical results work well for body surfaces with simple geometries, but as soon as the geometry becomes complicated, numerical approaches provide better basis for analysis. To apply to more complicated geometries, Lee and Leal [10] considered a matched asymptotic expansion method that used Green's integral representations of the velocity. Chadwick [1] takes this approach and matched Stokes and Oseen flow within a boundary integral formulation. It was found that the error is least if the matching boundary is on the body itself. Here, it is noted that this approach does not break down on the body boundary because in the formulation the oseenlet approximates to the stokeslet.

In this paper, the above mentioned approach in Chadwick [1] is tested by developing a BEM using point collocation weighting functions, linear shape functions, and two-point Gaussian quadrature with analytic removal of the Greens function singularity for the integrations. The Green's integral representation of oseenlets are distributed over the boundary surface. The BEM in this study compares favourably with Tritton experiment [17], analytical results of Lamb [9], Kaplun [7], Tomotika [16], and the numerical results of Yano and Kieda [19] for the drag coefficient. Hence, our method is simple yet robust in solving steady two-dimensional flow past a circular cylinder in an unbounded domain.

2. Formulation of Governing Equations

The motion of any continuous fluid is governed by the Navier-Stokes equation, and for a creeping flow, a linearisation of the Navier-Stokes equation yields Stokes and Oseen equation which govern a viscous fluid. Hence, away from a body surface the Oseen equation governs the flow in an outer region (see figure 1a) given by

$$\rho U \frac{\partial u_i}{\partial x_1} = -\frac{\partial p}{\partial x_i} + \mu \frac{\partial^2 u_i}{\partial x_j \partial x_j} + f_i \ , \tag{1}$$

$$\frac{\partial u_i}{\partial x_i} = 0 \ , \tag{2}$$

where Eq. (2) is the continuity equation, ρ is the density of the fluid, u_i is the velocity, p is the pressure, μ is the viscosity, U is the uniform stream velocity, and f_i is the applied force. Similarly, near the body Stokes equation governs the flow in an inner region (see figure 1b) given by

$$0 = -\frac{\partial p}{\partial x_i} + \mu \frac{\partial^2 u_i}{\partial x_j \partial x_j} + f_i \ , \tag{3}$$

$$\frac{\partial u_i}{\partial x_i} = 0 \ . \tag{4}$$

The viscous forces in Eq. (3) are dominant over the inertial forces, and by dimensionless analysis, the dimensionless Reynolds number tends to zero near the body with length dimension l and $Re = \frac{\rho U l}{\mu} \to 0$. To apply the Green's integral, it is supposed that an external force is exerted by the body on the fluid such that the applied force is f_i.

The work of Chadwick [1] considers a matched near-field region using Stokes flow and the far-field using Oseen flow. The common boundary where the matching takes effect, has L as the length dimension of the matched region and it is seen that $Re\frac{L}{l}$ is the error. So the error is reduced by choosing $L = l$ and Oseen flow assumed everywhere in the flow field, as shown in section 4.

3. Green's Function for Oseen and Stokes Equation

The oseenlet is the Green's function of the Oseen equation. In the limit as the Reynolds number tends to zero, the oseenlet approximates to the stokeslet which is the Green's function of the Stokes equation. The drag and lift oseenlet are

$$u_i^{(1)} = \frac{1}{2\pi\rho U}\left(\frac{\partial}{\partial x_i}\left(\ln r + e^{kx_1} K_0(kr)\right) - 2ke^{kx_1} K_0(kr)\delta_{i1}\right) \ , \tag{5}$$

$$p^{(1)} = -\frac{1}{2\pi}\frac{\partial}{\partial x_1}(\ln r) \ , \tag{6}$$

and

$$u_i^{(2)} = \frac{1}{2\pi\rho U}\varepsilon_{ij3}\frac{\partial}{\partial x_j}\left(\ln r + e^{kx_1}K_0(kr)\right) \ , \tag{7}$$

$$p^{(2)} = -\frac{1}{2\pi}\frac{\partial}{\partial x_2}(\ln r) \ , \tag{8}$$

where K_0 is the modified Bessel function of order zero, $k = \frac{\rho U}{2\mu}$, $\varepsilon_{ijk} = 1$ for $(i,j,k) = (1,2,3)$, $(2,3,1)$, $(3,1,2)$, $\varepsilon_{ijk} = -1$ for $(i,j,k) = (1,3,2)$, $(2,1,3)$, $(3,2,1)$, $\varepsilon_{ijk} = 0$ otherwise, and δ_{ij} is Kronecker delta such that $\delta_{ij} = 1$ for $i = j$ and $\delta_{ij} = 0$ for $i \neq j$.

To obtain the stokeslet from the oseenlet, consider $kr \to 0$, $e^{kx_1} = 1 + kx_1 + \mathcal{O}(k^2r^2)$ and $K_0(kr) = -\ln r + \mathcal{O}(r^2 \ln r)$. This will yield the drag and lift stokeslet respectively given as

$$u_i^{(1)} = \frac{1}{4\pi\mu}\left(\delta_{i1}\ln r - \frac{x_1x_i}{r^2}\right)(1 + \mathcal{O}(kr)) \ , \tag{9}$$

$$p^{(1)} = -\frac{1}{2\pi}\frac{x_1}{r^2} \ , \tag{10}$$

and

$$u_i^{(2)} = \frac{1}{4\pi\mu}\left(\delta_{i2}\ln r - \frac{x_2x_i}{r^2}\right)(1 + \mathcal{O}(kr)) + C_i, \tag{11}$$

$$p^{(2)} = -\frac{1}{2\pi}\frac{x_2}{r^2} \ , \tag{12}$$

where $C_i = \frac{\delta_{i2}}{4\pi\mu}$. Thus, up to order kr and a constant, the two-dimensional stokeslet is given by

$$u_i^{(m)} = \frac{1}{4\pi\mu}\left(\delta_{im}\ln r - \frac{x_mx_i}{r^2}\right)(1 + \mathcal{O}(kr)) + C_i^{(m)}, \tag{13}$$

$$p^{(m)} = -\frac{1}{2\pi}\frac{x_m}{r^2}, \tag{14}$$

where $C_i^{(m)} = \frac{\delta_{i2}\delta_{m2}}{4\pi\mu}$.

4. Green's Integral Formulation

4.1. Outer Region

Consider the space Σ enclosed by the boundary around and approaching the point x_i, the body boundary l_B, and the boundary on the far-field tending to an infinite distance away l_∞ (see figure 1). The Green's integral formulation for the Oseen flow [12] can be found by considering the integral,

$$\begin{aligned} &\int_\Sigma \left(-\rho U \frac{\partial u_i^{(m)}(z)}{\partial y_1} - \frac{\partial p^{(m)}(z)}{\partial y_i} - \mu \frac{\partial^2 u_i^{(m)}(z)}{\partial y_j \partial y_j} + f_i^{(m)}(z) \right) u_i(y) d\Sigma \\ &+ \int_\Sigma \left(-\rho U \frac{\partial u_i(y)}{\partial y_1} - \frac{\partial p(y)}{\partial y_i} + \mu \frac{\partial^2 u_i(y)}{\partial y_j \partial y_j} - f_i(y) \right) u_i^{(m)}(z) d\Sigma = 0 \ , \end{aligned} \tag{15}$$

where y_i is a vector position of the exterior domain integrated space Σ and in this case an area integral with $z_i = x_i - y_i$, so the differential equation for the Green's functions satisfies the conjugate Oseen equation since $\frac{\partial}{\partial y_j} = -\frac{\partial}{\partial x_j}$ and $f_i^{(m)}(z) = \delta(z)\delta_{im}$ where $\delta(z)$ is the Dirac delta function.

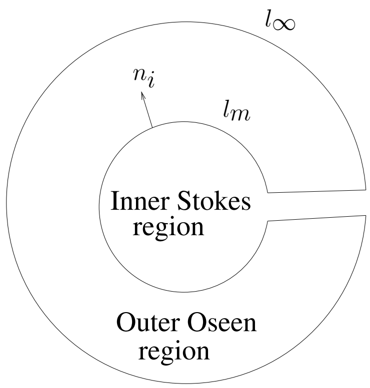

(a) Green's integral representation for outer Oseen flow

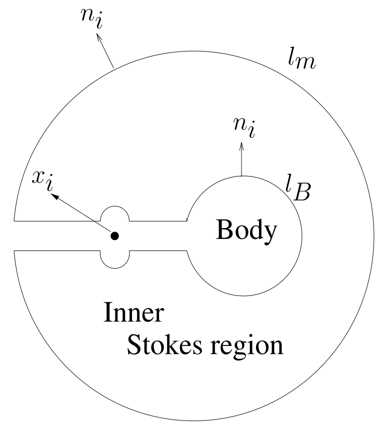

(b) Green's integral representation of inner Stokes flow

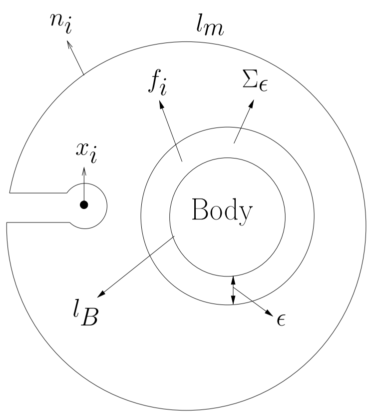

(c) Spatial distribution of point sources

Figure 1: Green's integral representation of a body in a near-field and far-field region

In the outer region, there is no body force so $f_i = 0$ and the point x_i is in the inner region, so there is no contribution $f_i^{(m)}(z)$ around the point x_i.

Rearranging Eq. (15) then gives

$$
\begin{aligned}
0 = & \int_\Sigma -\rho U \frac{\partial}{\partial y_1}\left(u_i^{(m)}(z) u_i(y)\right) d\Sigma \\
& - \int_\Sigma \frac{\partial}{\partial y_i}\left(p^{(m)}(z) u_i(y) + p(y) u^{(m)}(z)\right) d\Sigma \\
& + \int_\Sigma -\left(\mu \frac{\partial}{\partial y_j}\left(\frac{\partial u_i^{(m)}(z)}{\partial y_j} u_i(y)\right) - \mu \frac{\partial}{\partial y_j}\left(\frac{\partial u_i(y)}{\partial y_j} u_i^{(m)}(z)\right)\right) d\Sigma \ .
\end{aligned}
\tag{16}
$$

From the continuity equation (Eq. 2), it can be seen that $\mu \frac{\partial u_i^{(m)}}{\partial y_j} \frac{\partial u_i}{\partial y_j}$ cancel out in Eq. (16) by applying the divergence theorem. This then gives the Oseen's integral representation as

$$
\begin{aligned}
0 = & \int_{l_m} \left(\rho U u_i^{(m)}(z) u_i(y) n_1 + \left(p^{(m)}(z) u_i(y) + p(y) u_i^{(m)}(z)\right) n_i\right) dl \\
& + \int_{l_m} \mu \left(\frac{\partial u_i^{(m)}(z)}{\partial y_j} u_i(y) - \frac{\partial u_i(y)}{\partial y_j} u_i^{(m)}(z)\right) n_j dl
\end{aligned}
\tag{17}
$$

where l_m is the matching boundary. From Fishwick and Chadwick [3] the far field integral bounding the exterior domain Σ in the Oseen representation is zero, where the boundary of the domain in two-dimension is a closed curve.

4.2. Inner Region

The same approach used in the preceding section can be applied to give the Green's integral representation for the inner Stokes flow over a different domain integral (see figure 1b). Again there is no body force, so $f_i = 0$, but there is a contribution around the point x_i. Rearranging and simplifying Eq. (15) to get

$$
\begin{aligned}
-\int_\Sigma f_i^{(m)}(z) u_i^s(y) d\Sigma &= -\int_\Sigma \delta(z) \delta_{im} u_i^s(y) d\Sigma \\
&= -u_m^s(x) \ ,
\end{aligned}
$$

where $u_i^s(x)$, $p^s(x)$, $u_i^{(m)s}(x)$ and $p^{(m)s}(x)$ are the inner Stokes velocity and pressure, and inner Stokeslet velocity and pressure respectively. This then gives

$$-u^s_m(x) = \int_\Sigma -\rho U \frac{\partial}{\partial y_1}\left(u_i^{(m)s}(z)u_i^s(y)\frac{\partial}{\partial y_i}\left(p^{(m)s}(z)u_i^s(y) + p^s(y)u^{(m)s}(z)\right)\right) d\Sigma$$
$$+ \int_\Sigma -\mu \frac{\partial}{\partial y_j}\left(\left(\frac{\partial u_i^{(m)s}(z)}{\partial y_j}u_i^s(y)\right) + \left(\frac{\partial u_i^s(y)}{\partial y_j}u_i^{(m)s}(z)\right)\right) d\Sigma \ ,$$

$$\begin{aligned} u^s_m(x) = &- \int_{l_B}\left(p^{(m)s}(z)u_i^s(y) + p^s(y)u_i^{(m)s}(z)\right) n_i dl \\ &- \int_{l_B} \mu \left(\frac{\partial u_i^{(m)s}(z)}{\partial y_j}u_i^s(y) - \frac{\partial u_i^s(y)}{\partial y_j}u_i^{(m)s}(z)\right) n_j dl \\ &+ \int_{l_m}\left(p^{(m)s}(z)u_i^s(y) + p^s(y)u_i^{(m)s}(z)\right) n_i dl \\ &+ \int_{l_m} \mu \left(\frac{\partial u_i^{(m)s}(z)}{\partial y_j}u_i^s(y) - \frac{\partial u_i^s(y)}{\partial y_j}u_i^{(m)s}(z)\right) n_j dl \ . \end{aligned} \tag{18}$$

4.3. Matching Inner and Outer region

Here the inner and outer region are matched using Eq. (18) and Eq. (17), an error introduced as a result of the matching is giving next. In two-dimensions, the constant term $C_i^{(m)}$ give the leading order approximation to the velocity oseenlet $\left(1 + \mathcal{O}\left(\frac{1}{\ln kr}\right)\right) = \left(1 + \mathcal{O}\left(\frac{1}{\ln Re \frac{L}{l}}\right)\right)$ on the matching boundary where $r = \mathcal{O}(L)$. Hence, the matching integral in Eq. (18) is

$$\begin{aligned} &\int_{l_m}\left(p^{(m)s}(z)u_i^s(y) + p^s(y)u_i^{(m)s}(z)\right) n_i dl + \int_{l_m} \mu \left(\frac{\partial u_i^{(m)s}(z)}{\partial y_j}u_i^s(y) - \frac{\partial u_i^s(y)}{\partial y_j}u_i^{(m)s}(z)\right) n_j dl \\ &\quad \times \left(1 + \mathcal{O}\left(\frac{1}{\ln Re \frac{L}{l}}\right)\right) = - \int_{l_m}\left(\rho U u_i^{(m)}(z)u_i(y)n_1 + \left(p^{(m)}(z)u_i(y) + p(y)u_i^{(m)}(z)\right) n_i\right) dl \\ &\quad + \int_{l_m} \mu \left(\frac{\partial u_i^{(m)}(z)}{\partial y_j}u_i(y) - \frac{\partial u_i(y)}{\partial y_j}u_i^{(m)}(z)\right) n_j dl = 0 \ . \end{aligned} \tag{19}$$

So, to make the error as small as possible, we let $L = l$ and consider Oseen flow everywhere in the flow field.

5. Green's Integral for the Boundary Element Method

Now consider the space Σ enclosed by the boundary around the body boundary l_B and the boundary on the far-field: an infinite distance away l_∞. The body is represented by a distribution of forces f_i in the region Σ_ϵ which is a distance ϵ away from the body boundary l_B (see figure 1) and Eq. (17) then becomes (up to the error in the matching Eq. (19))

$$\begin{aligned}\int_\Sigma \Big(- f_i^{(m)}(z)u_i(y) + f_i(y)u_i^{(m)}(z)\Big) d\Sigma = & \int_\Sigma -\rho U \frac{\partial}{\partial y_1}\Big(u_i^{(m)}(z)u_i(y)\Big)\, d\Sigma \\ & - \int_\Sigma \frac{\partial}{\partial y_i}\left(p^{(m)}(z)u_i(y) + p(y)u^{(m)}(z)\right) d\Sigma \\ & - \int_\Sigma \left(\mu \frac{\partial}{\partial y_j}\left(\frac{\partial u^{(m)}(z)}{\partial y_j}u_i(y)\right) + \mu\frac{\partial}{\partial y_j}\left(\frac{\partial u_i(y)}{\partial y_j}u_i^{(m)}(z)\right)\right) d\Sigma \\ & = \int_{l_\infty}\left(\rho U u_i^{(m)}(z)u_i(y)n_1 + \Big(p^{(m)}(z)u_i(y) + p(y)u_i^{(m)}(z)\Big)\, n_i\right) dl \\ & - \int_{l_\infty}\mu\left(\frac{\partial u_i^{(m)}(z)}{\partial y_j}u_i(y) - \frac{\partial u_i(y)}{\partial y_j}u_i^{(m)}(z)\right) n_j dl = 0\ .\end{aligned} \tag{20}$$

We let

$$\int_{\Sigma_\epsilon} f_i(y)u_i^{(m)}(z)d\Sigma = \int_{l_B} F_i(y)u_i^{(m)}(z)dl\ , \tag{21}$$

on the body boundary so that as $\epsilon \to 0$, it gives the force on the body as

$$F_i(y) = \lim_{\epsilon\to 0}\int_0^\epsilon f_i(y)d\epsilon\ . \tag{22}$$

Therefore,

$$\begin{aligned} u_m &= \int_\Sigma \left(-f_i^{(m)}(z)u_i(y) + f_i(y)u_i^{(m)}(z)\right) d\Sigma \\ &= \int_{\Sigma_\epsilon} f_i(y)u_i^{(m)}(z)d\Sigma \end{aligned} \tag{23}$$

Hence,

$$u_m(x) = \int_{l_B} F_i(y)u_m^{(i)}dl \tag{24}$$

because by symmetry, $u_i^{(m)} = u_m^{(i)}$ from Eq. (5) and Eq. (7).
To proceed with the numerical method, Eq. (24) is discretised in the BEM given next.

6. Numerical Method

In the preceding section, the oseenlet is derived and given in Eq. (24) for a two-dimensional flow satisfying the Oseen equation for the far-field region and it was also shown above that in the matched region the oseenlet becomes the stokeslet. We shall compute the drag experienced by a circular cylinder in a steady flow in an unbounded domain. To do this, Eq. (24) is discretised using the BEM with a point collocation weighting function as seen in figure 2a, where $x_{\alpha i}$ is the position x_i of node α, the two nodal points are given by $x_{\alpha i}$ and $x_{\alpha+1i}$, while the midpoint between them is the collocation point. The collocation point is chosen not to lie on the nodes so that the Green's function singularity in the integral is more easily removed, because the singularity lies wholly within the element integration rather than divided across two elements. For ease of numerical formulation, the boundary is approximated by a linear rather than a curved variation, but as the number of nodes are increased the collocation points will move closer to the boundary and so this is not expected to be a problem.

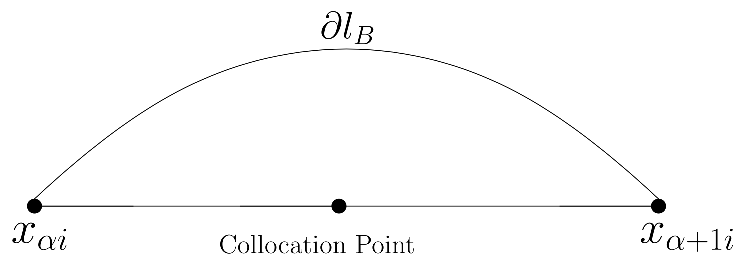

(a) Diagram showing collocation point

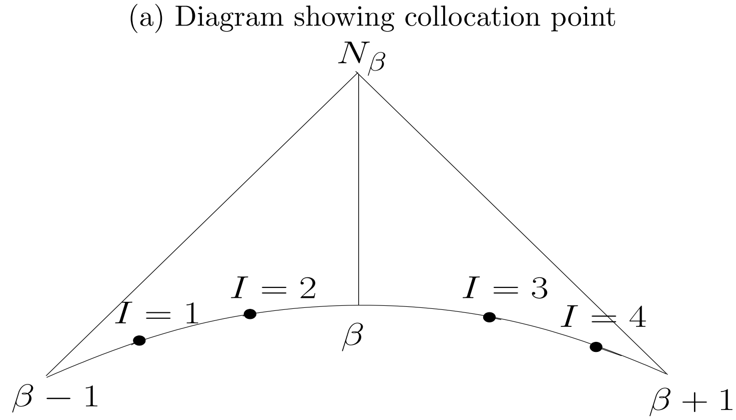

(b) Diagram showing Gaussian points

Figure 2: Figure showing the nodal points and Gaussian points used for collocation

In figure 2b, a two-point Gaussian quadrature is shown with Gaussian points $I = 1, 2$ for the integral from node $\beta - 1$ to β, and $I = 3, 4$ for the integral from node β to $\beta + 1$, N_β is the linear shape function at node β and gpw_I is the Gaussian point weight at point I. Hence Eq. (24) now becomes

$$\begin{aligned} u_i(x) &= \int_{l_B} N_\beta f_{\beta j} u_i^{(j)} dl \\ &= f_{\beta j} N_{\beta j} u_{ijI} gpw_I \ , \end{aligned} \quad . \tag{25}$$

where there are implied summations over $1 \leq \beta \leq n$ (for n nodes), over $1 \leq I \leq 4$ (for Gaussian points associated with node β (see figure 2), and over $1 \leq j \leq 2$ (for spatial dimension).
Also, u_{ijI} is the value of the oseenlet Green's function $u_i^{(j)}$ positioned at the Gaussian point I of node β, and determined at the node α. Hence, this collocation point method transforms the integral equation into a linear system of algebraic equations with a no slip boundary condition yielding

$$\mathbf{Af} = \mathbf{Y} \tag{26}$$

where $\mathbf{A}$ is a $2n \times 2n$ matrix, $\mathbf{f}$ is the force coefficient and $\mathbf{Y}$ is an n dimensional vector given by applying the boundary condition. Singularities from the Green's function which formed part of the matrix $\mathbf{A}$ are removed analytically. The full numerical formulation, including how the singularity is removed, is put in the appendix.

6.1. Flow Past a Circular Cylinder

As a first step of testing the BEM developed here, we begin by plotting streamlines for a flow past a circular cylinder. Although figure 3 and figure 4 do not give any quantifiable information, but they do give visualization for the streamlines in Reynolds number range 0.01 to 4 as expected from experiment, giving confidence in the formulation. It was noticed that for $Re = 0.01$, the streamlines align (see figure 3). Whereas when the Reynolds number is increase to about 4, eddies began to form near the cylinder (see figure 4) which is expected from experiment [18]. This is benchmark against analytical results for low Reynolds number below 0.1, given accuracy of 1%.

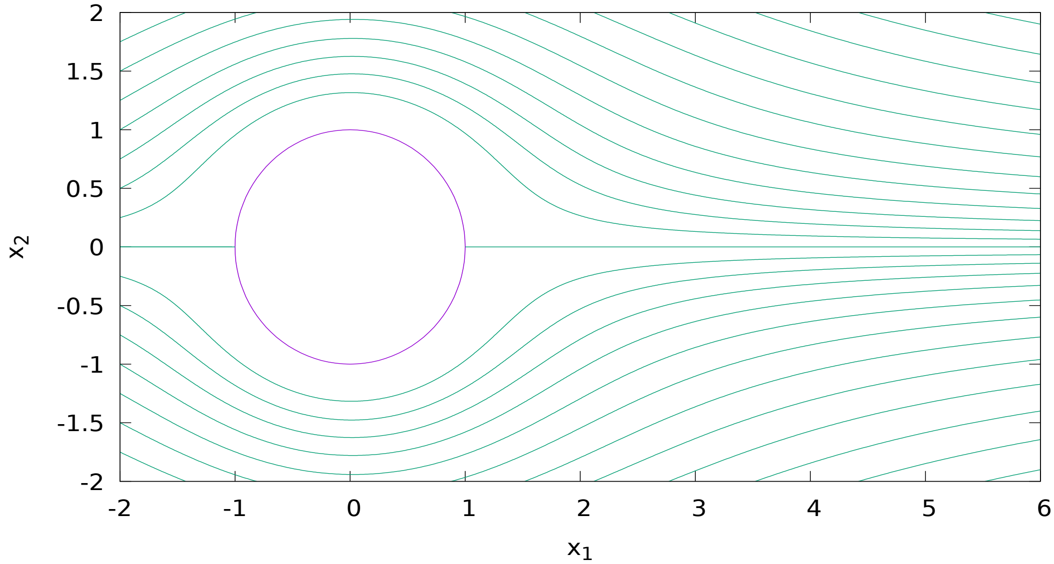

Figure 3: Streamlines of steady flow past a circular cylinder at $Re = 0.01$ in an unbounded domain.

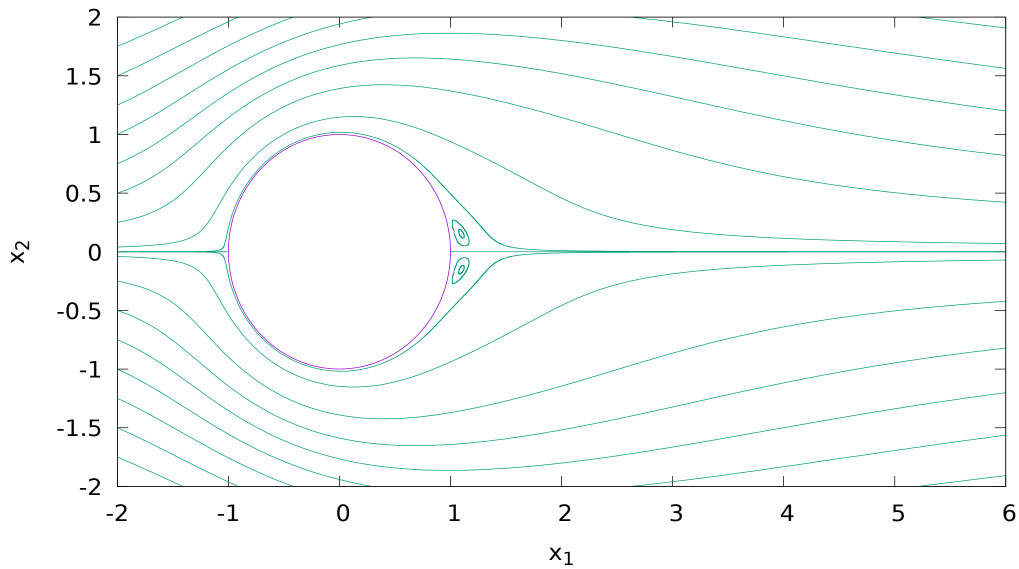

Figure 4: Streamlines of steady flow past a circular cylinder at $Re = 4$ in an unbounded domain which formed eddies

To validate against existing results, the drag coefficient C_D from the BEM presented in this study is compared against results of Lamb [9] Eq. (27), Tomotika [16] Eq. (28), Kaplun [7] Eq. (29), experimental results of Tritton [17], and numerical results of Yano and Kieda [19] all for a Reynolds number Re ranging between 0 and 4 (see figure 5). The approximation of the drag coefficients for the various listed results are

$$\text{Lamb:} \quad C_D = \frac{4\pi}{ReT_1} \tag{27}$$

$$\text{Tomotika:} \quad C_D = \frac{4\pi}{ReT_1}\left(1 - T_2\right) \tag{28}$$

$$\text{Kaplun:} \quad C_D = \frac{4\pi}{ReT_1}\left(1 - 0.87T_1^{-2}\right) \tag{29}$$

$$\text{Lee and Leal:} \quad C_D = \frac{-2\pi}{Re\ln(2Re)}\left(1 + \frac{1}{\ln(2Re)}\left(\frac{1}{2} - \gamma + \ln 4\right)\right) \tag{30}$$

where the Reynolds number Re is defined by $Re = \frac{aU}{\nu}$, with a as the cylinder radius and $\nu = \frac{\mu}{\rho}$ is the kinematic viscosity with μ as the dynamic viscosity of the ambient fluid. The parameter $T_1 = \left(\frac{1}{2} - \gamma - \log\frac{Re}{4}\right)^{-1}$, $T_2 = \frac{Re^2}{8T_1}\left(T_1^2 - \frac{1}{2}T_1 + \frac{5}{16}\right)$ with $\gamma = 0.577216...$ as the Euler constant.

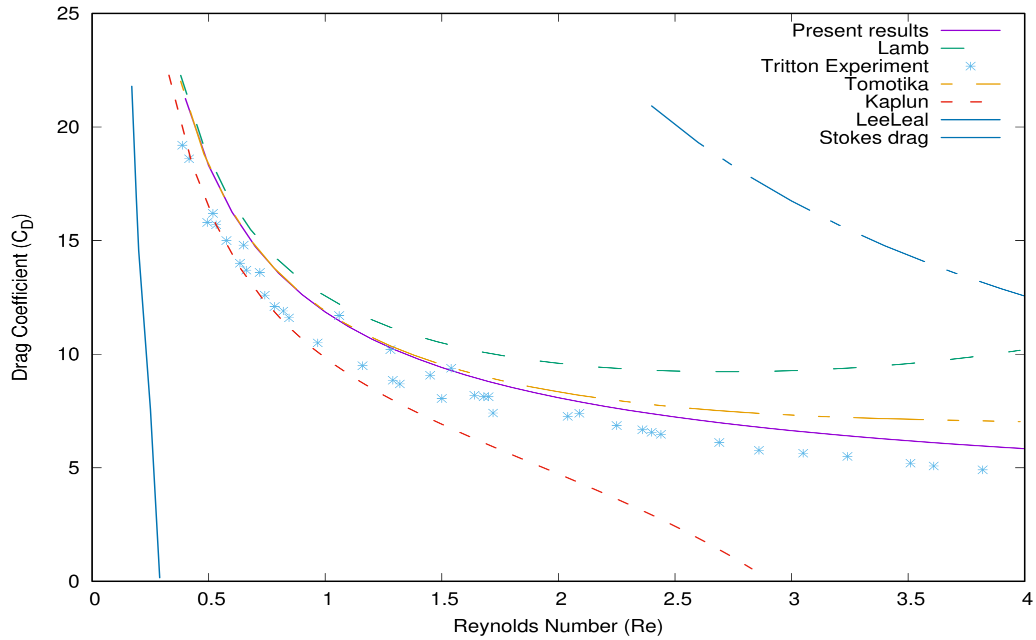

Figure 5: Drag coefficient C_D are plotted against the Reynolds number ($0 < Re < 4$)

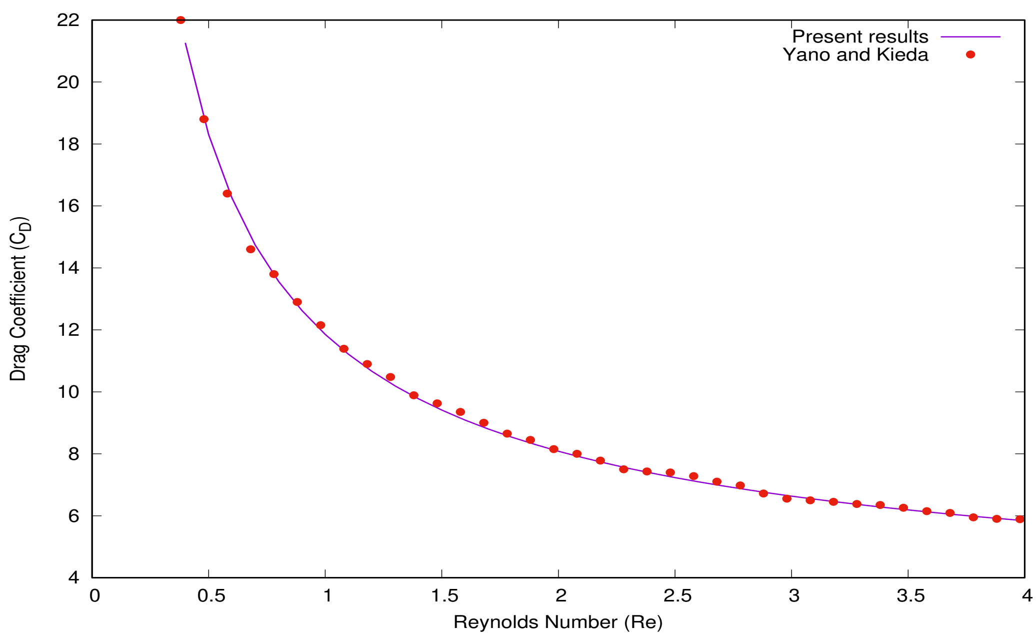

Figure 6: Comparing present result with Yano and Kieda [19]

In figure 5, the drag coefficient is plotted against the Reynolds number. Lamb's [9] and Kaplun's [7] vary increasingly as the Reynolds number is increased beyond 1 ($Re > 1$), and the present results together with Yano and Kieda [19] give the closest match to Tritton's experiment [17]. The Stokes drag shows clearly that the velocity diverges when considering a 2D flow past a circular cylinder in an unbounded domain as expected from Stokes paradox. When considering the Reynolds number below 1 ($Re < 1$), it can be seen that the difference in the results are not significant (see figure 5), they all aligned with experiment at very low Reynolds number. Analytic result of Kaplun and Lagerstrom actually diverge to a negative value as the Reynolds number increase above 2.9 ($Re > 2.9$).

Furthermore, the present result is compared with the discrete singularity result of Yano and Kieda [19] at similar range of Reynolds number (see figure 6). In their formulation, Yano and Kieda choose a specific points within a body surface and distributed oseenlets, sink, and sources within a body. It is unclear on how to extend the work of Yano and Kieda [19] to a general closed body as their method specifically tailored to the circular cylinder, whereas the method presented here is straightforward to apply for any closed body.

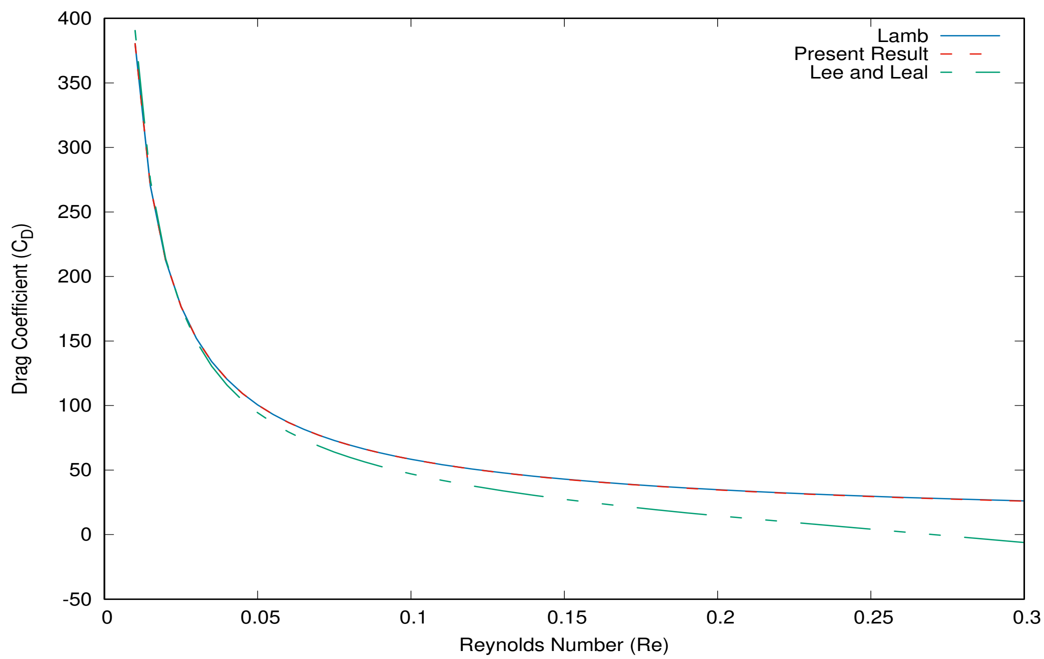

Figure 7: Comparisons of drag coefficient for very low Re in range $0.01 \le Re \le 0.3$ for Lamb, Lee and Leal/Proudman and Pearson, and our BEM

Observe that in figure 7, Lamb [8] and present result appear the same in the range $0.01 < Re < 0.3$, but the result of Lee and Leal [10] begin to diverge as the Reynolds number increases. The result of Lee and Leal diverges to negative values when $Re > 0.28$.

6.2. Flow Past an Elliptical Cylinder

The BEM developed here is also tested on elliptical cylinder at different angle of inclination ranging from $0°$ to $90°$. In figures 8 and 9, we consider the thickness ratio of the elliptic cylinder denoted by t, which is the ratio of the minor axis to major axis of the ellipse. The figures are shown for the drag coefficient against angle of attack α, varying from $0°$ to $90°$ for the ellipse. In figure (8), the Reynolds number is set to $Re = 0.1$. When $t = 1$, it can be seen that the drag coefficient remains constant irrespective of the angle α, it is true because that gives a circular cylinder. When $t = 0.1$ and $t = 0.5$ it can be seen that the drag coefficient reaches optimal when the angle is $90°$, this is expected when compared to the results of Yano and Kieda [19]. In figure 9, the Reynolds number is now set to $Re = 1$ with the same angle of attack as in figure (8), it can be seen that the drag coefficient here is lower but it also reaches optimal drag values when the angle is 90°. The drag coefficient here is lower than when the Reynolds number is $Re = 0.1$ which is expected.

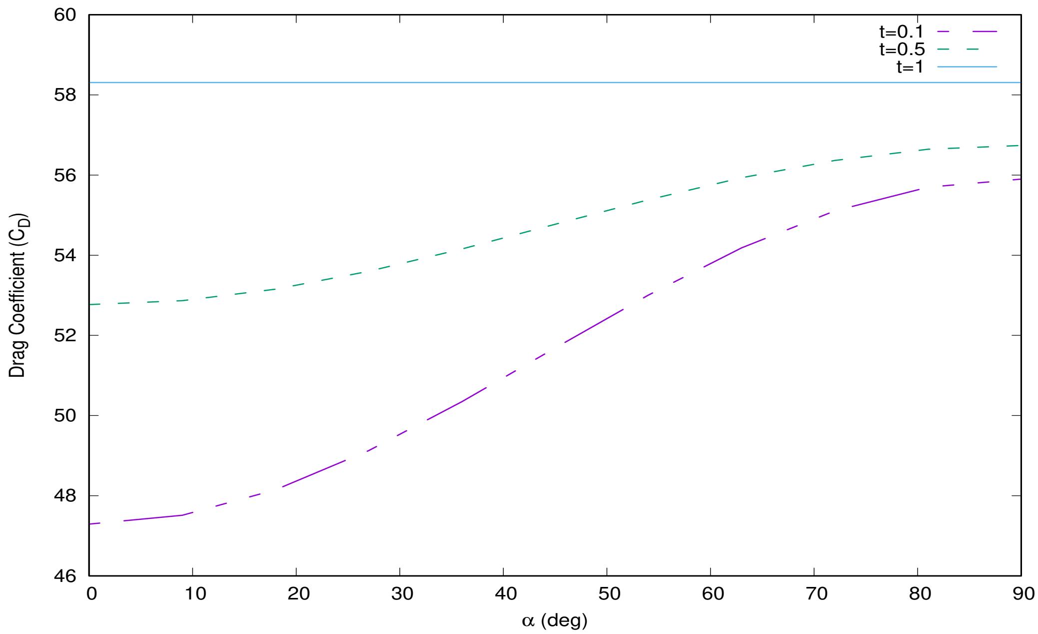

Figure 8: Drag coefficient C_D for an inclined elliptical cylinder at Reynolds number $Re = 0.1$ plotted against angle α for present result

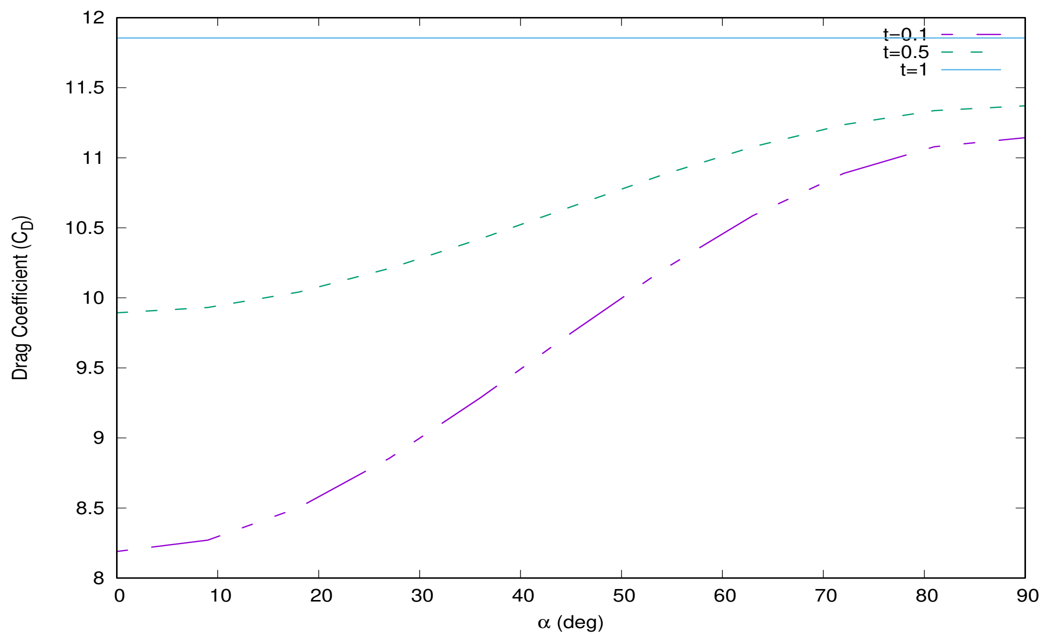

Figure 9: Drag coefficient C_D for an inclined elliptical cylinder at Reynolds number $Re = 1$ plotted against angle α for present result

Hence matching Stokes and Oseen equation in a boundary element formulation using point collocation weighting functions, linear shape functions, two-point Gaussian quadrature with analytic removal of the Green's function singularity for the integrations give good results compared to other methods discussed.

7. Conclusion

A BEM for solving a two-dimensional steady flow past a circular cylinder has been presented. Our results agree against the other benchmark results and are an improvement at the higher Reynolds number range up to 4. So our representation gives a good description of the flow field even outside the low-Reynolds number region of $Re < 1$. In particular, it gives better results than the matched asymptotic method of Kaplun [7]. The present result is also able to deal with complicated geometries. For future work, consider biological fluid dynamics and the modelling of the motion of macroscopic organisms, microscopic organisms, and micro robots. Such an organism can be represented by a generic closed swimming body in a quasi-steady problem by using this boundary element method.

8. Appendix

8.1. Numerical Formulation

The discretisation leading to Eq. (25) is

$$\begin{aligned} u_i &= \int_{\partial\Sigma_0} f_j u_{ij} dl' \\ &= \int_{\partial\Sigma_0} N_\beta f_{\beta j} u_{ij} dl' \end{aligned} \tag{31}$$

where $N_\beta(\underline{x}')$ is the shape function, $u_{ij}(\underline{x}-\underline{x}')$ is the Green's function evaluated at $\underline{x}'$, $\underline{x}'$ is a position on the domain $\partial\Sigma_0$, dl' is an element of the length integration variable. $1 \leq i,\ j \leq m$, where m is the size of the dimensional space and $1 \leq \beta \leq n$ represents the descritisation points.
On the boundary,

$$\int_{\partial\Sigma_0} W_\alpha u_i dl = \int_{\partial\Sigma_0} W_\alpha \int_{\partial\Sigma_0} N_\beta f_{\beta j} u_{ij} dl' dl$$

where $1 \leq \alpha \leq n$, $W_\alpha(\underline{x})$ is the weighting function at node α integrated over $\underline{x}$ position on Σ element of length dl.
As a result,

$$u_{\alpha i} = u_{\alpha\beta ij} f_{\beta j} \tag{32}$$

where

$$u_{\alpha i} = \int_{\partial\Sigma_0} W_\alpha u_i dl$$

$$u_{\alpha\beta ij} = \int_{\partial\Sigma_0} W_\alpha \int_{\partial\Sigma_0} N_\beta u_{ij} dl' dl\ .$$

We need to renumber (32) so that we can put it into a matrix form in order to solve it in a matrix solver.
Hence, we renumber to $\alpha^* = \alpha + (i-1)n$, and $\alpha = \alpha^* - (i-1)n$, with $\beta^* = \beta + (j-1)n$, and $\beta = \beta^* - (j-1)n$, where $1 \leq \alpha^*, \beta^* \leq m \times n$, $i = 1 + \left(\frac{\alpha^*}{n+1}\right)_{\text{integer division}}$, and $j = 1 + \left(\frac{\beta^*}{n+1}\right)_{\text{integer division}}$.
In renumbered form, (32) becomes

$$u_{\alpha^*} = u_{\alpha^*\beta^*} f_{\beta^*}, \tag{33}$$

and the matrix we require is

$$f_{\beta^*} = u^{-1}_{\alpha^*\beta^*} u_{\alpha^*}. \tag{34}$$

Consider a uniform flow δ_{i1} past a two dimensional ($m = 2$) circular cylinder of radius 1, given that the weighting function is the collocation point and the shape function is a linear two-point Gaussian, we want to evaluate u_{α^*} $[u_{\alpha i}]$

$$\begin{aligned} u_{\alpha i} =& \int_{\partial\Sigma_0} W_\alpha u_i dl \\ =& \int_{\partial\Sigma_0} \delta(\underline{x}_{\alpha+\frac{1}{2}}) u_i dl \\ =& u_i(\underline{x}_{\alpha+\frac{1}{2}}) \end{aligned}$$

The last term on the above equation is the mid point shown in figure 2a . For clarity purposes, $\underline{x}_\alpha/x_{\alpha i}$ is a position vector x_i of node α and $\underline{x}_{\alpha+\frac{1}{2}}/x_{\alpha+\frac{1}{2}i}$ is the position vector x_i of the mid-point between nodes α and $\alpha+1$. $x_{\alpha+\frac{1}{2}i} = \frac{1}{2}\left(x_{\alpha i} + x_{\alpha+1i}\right)$ is the mid-point with the boundary condition $u_i|_{\partial\Sigma_0} = -\delta_{i1}$, which means that $u_{\alpha i} = u_{\alpha+\frac{1}{2}i} = -\delta_{i1}$. We also want to evaluate the Non-degenerative singularity case, first, for $\alpha \neq \beta - 1, \beta$ which gives

$$\begin{aligned} u_{\alpha\beta ij} =& \int_{\partial\Sigma_0} W_\alpha \int_{\partial\Sigma_0} N_\beta u_{ij} dl' dl \\ =& \int_{\partial\Sigma_0} N_\beta u_{ij}(\underline{x}_{\alpha+\frac{1}{2}} - \underline{x}) dl' \\ =& N_{\beta I} gpw_I u_{ij}(\underline{y}), \end{aligned} \tag{35}$$

where $y_i = x_{\alpha+\frac{1}{2}i} - x_{\beta i I}$, $N_{\beta I}$ is the shape function at Gaussian points I, $N_{\beta I} = \left(\frac{1}{2} - \frac{1}{2\sqrt{3}}, \frac{1}{2} + \frac{1}{2\sqrt{3}}, \frac{1}{2} + \frac{1}{2\sqrt{3}}, \frac{1}{2} - \frac{1}{2\sqrt{3}}\right)$, gpw_I is the Gaussian point weight at point I with $gpw_I = \left(\frac{l^-}{2}, \frac{l^-}{2}, \frac{l^+}{2}, \frac{l^+}{2}\right)$ where the length between nodes is given as $l^- =\mid x_{\beta i} - x_{\beta+1i} \mid$, and $l^+ =\mid x_{\beta+1i} - x_{\beta i} \mid$. The four different Gaussian points are illustrated in figure 2b, $x_{\beta iI}$ is the position x_i of Gaussian point I

of node β such that

$$
\begin{aligned}
x_{\beta iI} =& \frac{x_{\beta-1i}+x_{\beta i}}{2} - \frac{x_{\beta i}-x_{\beta-1i}}{2\sqrt{3}}, \\
& \frac{x_{\beta-1i}+x_{\beta i}}{2} + \frac{x_{\beta i}-x_{\beta-1i}}{2\sqrt{3}}, \\
& \frac{x_{\beta+1i}+x_{\beta i}}{2} - \frac{x_{\beta+1i}-x_{\beta i}}{2\sqrt{3}}, \\
& \frac{x_{\beta+1i}+x_{\beta i}}{2} + \frac{x_{\beta+1i}-x_{\beta i}}{2\sqrt{3}}
\end{aligned}
$$

$u_{ij}(y)$ is the stokeslet given by

$$
u_{ij}(y) = \frac{Re}{4\pi}\left(\delta_{ij}\ln r - \frac{y_i y_j}{r^2}\right), \tag{36}
$$

and where $r = +\sqrt{y_i y_j}$.
We also wish to evaluate the degenerate case with singularities for $i = j$, $\alpha = \beta$. In this case, the singularity needs to be removed

$$
\begin{aligned}
u_{\alpha\beta ij} =& \int_{\partial\Sigma_0} N_\beta u_{ij} dl' \\
=& \int_{l^-} N_\beta u_{ij} dl' + \int_{l^+} N_\beta \left(u_{ij} - u_{ij}^{s^*}\right) dl' + \int_{l^+} N_\beta u_{ij}^{s^*} dl' \\
=& N_{\beta 1} u_{ij}(\underline{y}) gpw_1 + N_{\beta 2} u_{ij}(\underline{y}) gpw_2 + N_{\beta 3}\left(u_{ij} - u_{ij}^{s^*}\right) gpw_3 \\
& + N_{\beta 4}\left(u_{ij} - u_{ij}^{s^*}\right) + \int_{l^+} N_\beta u_{ij}^{s^*} dl',
\end{aligned}
$$

where s^* denotes a singularity, and when the singularity is solved analytically, it becomes

$$
u_{ij} = \frac{Re}{4\pi}\delta_{ij}\ln r. \tag{37}
$$

Thus,

$$
\begin{aligned}
\int_{l^+} N_\beta u_{ij}^{s^*} dl' =& \frac{Re}{4\pi}\int_{l^+} N_\beta \ln r dl' \\
=& \frac{Re}{4\pi}\delta_{ij}\left(\frac{l^+}{2}\left(\ln\left(\frac{l^+}{2}\right) - 1\right)\right),
\end{aligned} \tag{38}
$$

and when $i = j$ and $\alpha = \beta - 1$, then

$$
\begin{aligned}
u_{\alpha\beta ij} =& \int_{\partial\Sigma_0} N_\beta u_{ij} dl' \\
=& \int_{l^-} N_\beta \left(u_{ij} - u_{ij}^{s^*}\right) dl' + \int_{l^-} N_\beta u_{ij}^{s^*} dl' + \int_{l^+} N_\beta u_{ij} dl' \\
=& N_{\beta 1} \left(u_{ij} - u_{ij}^{s^*}\right) gpw_1 + N_{\beta 2} \left(u_{ij} - u_{ij}^{s^*}\right) gpw_2 \\
&+ \int_{l^-} N_\beta u_{ij}^{s^*} dl' + N_{\beta 3} u_{ij} gpw_3 + N_{\beta 4} u_{ij} gpw_4
\end{aligned}
\tag{39}
$$

so that we have

$$
\begin{aligned}
\int_{l^-} N_\beta u_{ij}^{s^*} dl' =& \frac{Re}{4\pi} \delta_{ij} \int_{l^-} N_\beta \ln r dl' \\
=& \frac{Re}{4\pi} \delta_{ij} \left(\frac{l^-}{2} \left(\ln \left(\frac{l^-}{2} \right) - 1 \right) \right).
\end{aligned}
\tag{40}
$$

To find the solution to (39), we shall find the velocity in the domain, pressure coefficient on the cylinder, as well as the drag coefficient.
In the fluid, the velocity becomes

$$
\begin{aligned}
u_i(\underline{x}) =& \int_{\partial\Sigma_0} N_\beta f_{\beta j} u_{ij} dl' \\
\approx& N_{\beta I} f_{\beta j} u_{ij} (\underline{x} - \underline{x}_{\beta I}) gpw_I.
\end{aligned}
\tag{41}
$$

By linear superposition,

$$
p(\underline{x}) \approx f_{\beta j} N_{\beta I} p_j (\underline{x} - \underline{x}_{\beta I}) gpw_I \tag{42}
$$

where p_j is the Stokes pressure given by

$$
p_j = \frac{-1}{2\pi} \frac{y_j}{r^2} \tag{43}
$$

On the cylinder, the pressure at node β is

$$
p_\beta = -f_{\beta j} n_j |_\beta \tag{44}
$$

where $n_j|_\beta = x_{\beta j}$.
The force coefficient:

$$\begin{aligned} C_i &= \int_{\partial\Sigma_0} f_i dl \\ &\approx \int_{\partial\Sigma_0} N_\beta f_{\beta i} dl \\ &\approx f_{\beta i} N_{\beta i} gpw_I \qquad (45) \\ &= f_{\beta i}\left(s_\beta \left(\frac{l^+ + l^-}{2}\right)\right) \\ &= f_{\beta i} s_\beta L \qquad (46) \end{aligned}$$

where $s_\beta = 1$ is the summation vector and $l = \frac{l^+ + l^-}{2}$ for n nodes. When $l^- = l^+ = l$, then $l = \frac{2\pi}{n}$, and

$$\begin{aligned} C_i &= \frac{2\pi}{n} f_{\beta i} s_\beta \\ &= \frac{2\pi}{n} \sum_{\beta=1}^{n} f_{\beta i}. \qquad (47) \end{aligned}$$

Where $i = 1$, equation (47) describes the drag coefficient, while for $i = 2$, it describes the lift coefficient.
These numerical results must be tested against known analytical solutions. The analytical solutions are

$$u_i = \frac{8\pi}{Re} u_{i1} + \frac{2\pi}{Re} u_{i1,jj}$$

and

$$p = \frac{8\pi}{Re} p_1 + \frac{2\pi}{Re} p_{1,jj},$$

so the analytical solution is represented by a drag stokeslet of strength $\frac{8\pi}{Re}$ plus a quadrupole giving drag, such that

$$C_D = \frac{8\pi}{Re} \ . \qquad (48)$$

Recall that the stokeslet velocity and pressure are given as

$$u_{ij} = \frac{Re}{4\pi}\left(\delta_{ij} \ln r - \frac{y_i y_j}{r^2}\right),$$

$$p_j = -\frac{1}{2\pi}\frac{y_j}{r^2},$$

and the Stokes equation given by

$$0 = -p_{,i} + \frac{1}{Re}u_{i,jj}$$

Therefore, the velocity is shown to be a uniform stream, given by

$$\begin{aligned}
u_i|_{r=1} &= \left[\frac{8\pi}{Re}u_{i1} + 2\pi p_{1,i}\right]_{r=1} \\
&= \left[\frac{8\pi}{Re}\left(\frac{Re}{4\pi}\left(\delta_{ij}\ln r - \frac{y_i y_j}{r^2}\right)\right) + 2\pi\left(-\frac{1}{2\pi}\frac{y_j}{r^2}\right)_{,i}\right]_{r=1} \\
&= \left[2\delta_{i1}\ln r - \frac{2y_i y_1}{r^2} - \frac{r^2\delta_{i1} - y_i 2r y_i/r}{r^4}\right]_{r=1} \\
&= \left[2\delta_{i1}\ln r - \frac{2y_i y_1}{r^2} - \frac{\delta_{i1}}{r^2} + \frac{2y_i y_1}{r^4}\right]_{r=1} \\
&= -\delta_{i1}.
\end{aligned}$$

Acknowledgement

This work is supported by the Nigerian government and the University of Jos, Plateau State, Nigeria.

References

[1] Chadwick, E.A.: The Far-field Greens Integral in Stokes Flow from the Boundary Integral Formulation. *CMES.* **96(3)**, (2013) 177-184.

[2] Cheng, A.H-D. and Cheng, D.T.: Heritage and early history of the boundary element method. *Engineering Analysis with Boundary Elements* **29(3)** (2005), 268-302.

[3] Fishwick, N. and Chadwick, E.: The evaluation of the far-field integral in the Greens function representation for steady Oseen flow. *Physics of Fluids* **18(11)** (2006), 113101.

[4] Hao, W., Hu, B., Li, S., and Song, L.: Convergence of boundary integral method for a free boundary system. *Journal of Computational and Applied Mathematics* **334** (2018), 128-157.

[5] Imai, I.: On the asymptotic behaviour of viscous fluid flow at a great distance from a cylindrical body, with special reference to Filons paradox. *Proc. Roy. Soc. Lon. A.* **208(1095)** (1951), 487-516.

[6] Imai, I.: A new method of solving Oseen's equation and it's application to the flow past an elliptic cylinder. *Proc. Roy. Soc. Lon. A.* **224** (1954), 141-160.

[7] Kaplun S.: Low Reynolds number flow past a circular cylinder. *J. of math. and mech.* (1957), 595-603.

[8] Lamb, H.: On the uniform motion of a sphere through a viscous fluid. *The London, Edinburgh, and Dublin Philosophical Magazine and Journal of Science* **21(121)** (1911) 112-121.

[9] Lamb H.: Hydrodynamics. *Cambridge University Press* (1932).

[10] Lee, S.H. and Leal, L.G.: Low-Reynolds-number flow past cylindrical bodies of arbitrary cross-sectional shape. *J. fluid mech.* **164** (1986), 401-427.

[11] Oseen, C.W.: Uber die Stokes sche Formel und Uber eine verwandte Aufgabe in der Hydrodynamik Arkiv Mat. *Astron. och Fysik,* **6(1)** (1910).

[12] Oseen, C.W.: Neuere methoden und ergebnisse in der hydrodynamik. *Leipzig: Akademische Verlagsgesellschaft mb H.* (1927).

[13] Proudman, I. and Pearson, J.R.A.: Expansions at small Reynolds numbers for the flow past a sphere and a circular cylinder. *J. fluid mech.* **2(3)** (1957), 237-262.

[14] Smith, D.J. and Gaffney, E.A. and Blake, J.R. and Kirkman-Brown, J.C.: Human sperm accumulation near surfaces: a simulation study. *J. fluid mech.* **621** (2009), 289-320.

[15] Stokes, G.G.: *On the effect of the internal friction of fluids on the motion of pendulums.* Pitt Press Cambridge (1851).

[16] Tomotika, S. and Aoi, T.: An expansion formula for the drag on a circular cylinder moving through a viscous fluid at small Reynolds numbers. *The Quarterly Journal of Mechanics and Applied Mathematics* **4(4)** (1951), 401-406.

[17] Tritton, D.J.: Experiments on the flow past a circular cylinder at low Reynolds numbers *J. fluid mech.* **6(4)** (1959), 547-567.

[18] Van Dyke, M.: An album of fluid motion *Parabolic Press* (1982).

[19] Yano, H. and Kieda, A.: An approximate method for solving two-dimensional low-Reynolds number flow past arbitrary cylindrical bodies *J. fluid mech.* **97(1)** (1980), 157-179.